Numerical Methods in Civil Engineering, 9-4 (2025) 74-95

Numerical Methods in Civil Engineering

Journal Homepage: https://nmce.kntu.ac.ir/

Numerical Modeling of 3D Flow Field in a Seawater Intake System Study Case: Bandar Abbas Seawater Desalination Plant

Akbar Safarzadeh*, Mehdi Shafieefar**

ARTICLE INFO

RESEARCH PAPER

Article history:
Received:
October 2024
Revised:
April 2025
Accepted:
May 2025

Keywords:
Pump Intake;
Desalination Plant;
CFD;
Swirl Angle;
Guide Vane;

Abstract:

This paper presents the findings of CFD analyses conducted to simulate the flow in the intake system of the Bandar Abbas seawater desalination plant. To accurately simulate turbulent flow with sudden strain rate, separating and circulating zones within the basin, the Reynolds Stress Model (RSM) was used as the turbulence closure model. The effects of different pump operation scenarios on the hydromechanics of the forebay area and pump bays were investigated. Flow streamlines, velocity distribution, and swirl angle values at different planes were used to evaluate the performance of the intake system under symmetric and asymmetric operating modes. The results revealed that the initial design geometry of the basin had multiple unfavorable dead zones along the forebay, and complex flow structures in the forebay led to flow non-uniformity and development of separation zones along the pump bays. The asymmetric operation of the intake system resulted in even more unfavorable flow conditions. However, modifying the basin's geometry by adding three diverging guide vanes at the forebay inlet resulted in a more proper flow pattern compared to the flow in the intake system with the initial geometry. The modified geometry eliminated all dead zones along the forebay and created uniform flow along all pump bays without any separation zones. In the base geometry, the Sym-3 and Asym-5 scenarios achieved the highest uniformity indices (U.I.) of 110% and 130%, respectively. In contrast, in the modified geometry, the U.I. values for the Sym-3 and Asym-5 operational scenarios were measured at 24% and 27%, respectively. This modified geometry met all recommendations of the ANSI/HI 9.8-2012 standard.

1. Introduction

The oceans contain more than 97% of Earth's water, representing a vast and renewable resource that is resilient to drought. In light of climate change and the increasing frequency of droughts and floods, desalination offers a reliable means of converting seawater into fresh water, thereby securing an adequate supply for both human needs and industrial applications. Desalination is an environmentally sustainable solution that contributes to the circular water economy, addressing water scarcity especially in arid regions and areas with limited freshwater resources, such as the Middle East. By converting seawater into potable water, desalination not only helps meet the growing demand for fresh water but also promotes efficient water use and management, supporting both ecosystems and communities. This technology plays a crucial role in enhancing water security and resilience against climate variability. Approximately 44% of the world's desalination capacity is situated in North Africa and the Middle East, with an estimated annual growth rate of 7-9% [1]. Seawater desalination plants require an intake system capable of providing a reliable quantity and consistent quality of clean water with a minimum environmental impact. Water intake methods can generally be divided into two main types: surface intakes, also known as open intakes, which draw water from the ocean's upper layers, and subsurface intakes, where water is extracted from beach wells, infiltration galleries, or other sites beneath the seabed [2, 3].

* *Corresponding author: Professor, Department of Civil and Environmental Engineering, Tarbiat Modares University, Tehran, Iran. E-mail: safarzadeh@modares.ac.ir*
** *Professor, Department of Civil and Environmental Engineering, Tarbiat Modares University, Tehran, Iran. E-mail: Shafiee@modares.ac.ir*

https://doi.org/10.61186/NMCE.2410.1078

Surface intakes are used in locations where the water depth is sufficient. The main components of open intakes include: (1) Intake pipes or channels, through which seawater is drawn into the system, (2)a large basin or pool built near the shore that is connected to the seawater by the pipeline or channel, (3) Screening devices, which are used to filter out debris, such as seaweed, fish or other marine life, that can clog or damage the intake system, (4) Pump stations- once the seawater has been screened for unwanted solids, it is pumped into the desalination system. A group of pumps located at the terminus of the parallel bays, divided by vertical walls, work together to convey raw water from the basin to the desalination plant, constituting the pump system. Water intake stations that manage inflows to the plants are essential for ensuring the smooth operation of the processes. In the forebay of a seawater intake system, the presence of spiral and large-scale reverse flows can significantly impact the conditions at the pump's inlet. The key aim of designing both the forebay and the pump intake is to provide a steady, uniform, and swirl-free flow into the impeller. Achieving these ideal hydrodynamic conditions is dependent on the proper design of the basin geometry and according to Figure (1), ANSI/HI 9.8-2012 recommends basin design criteria considering the following points [4]:

To avoid any cross-flows at the entrance of the pump bays, the flow in the basin must be directed appropriately. Additionally, the supply boundary of the basin must be symmetrical in relation to the structure's centreline, ensuring that flow patterns approaching any of the pumps are equally balanced. A good rule of thumb is to keep cross-flow velocities (V_c) below 50 percent of the pump bay inlet velocity. To ensure channel flow uniformity and appropriate approach velocity, the pump bay should have sufficient width, depth, and length. It is important to note that the maximum allowable pump approach velocity (V_x) is 0.5 m/s. Velocities at points in the throat must be within 10% of the cross-sectional area average velocity [4]. To avoid the formation of significant free-surface vortices, the necessary minimum submergence is connected to the diameter of the inlet bell (or pipe).

Surface and sub-surface vortices induced by fluid passing through obstructions, may form in the pump bay and around the intake pipe. These vortical formations that are pulled into the pipe can capture air pockets and debris from the surface, which reduces the effective cross-section of the pipe flow, diminishes pump efficiency, and may lead to vibrations throughout the entire system. (Tsou et al., 1994). As a result, they increase the maintenance costs. The swirl angle (θ) is defined as a function of the ratio between tangential velocity (v_θ) and axial velocity (v_z), as follows:

$$\theta = tan^{-1}(v_\theta / v_z) \quad (1)$$

Mitra et al. suggested the following equation to calculate the swirl angle using results of the CFD analysis [5]:

$$\theta = tan^{-1}(R\omega / v_z), \omega = \frac{\int_A (r \times v)(\rho v \cdot \hat{n} dA)}{\int_A r^2 (\rho v \cdot \hat{n} dA)} \quad (2)$$

where, R is the pipe inlet radius, ω is the bulk angular velocity, r is the position vector measured from the pipe centre, v is the local velocity vector, $\hat{n}$ is the unit vector and A is the flow area. The swirl angle parameter represents the inherent rotation of flow entering the pump, and it is desirable to maintain a relatively low magnitude for efficient pump performance. The ANSI/HI 9.8-2012 standard specifies that the maximum swirl angle of flow entering the pump should not exceed 7 degrees. Gordon identified four primary factors that contribute to vortex formation in intake systems: the geometry of the approach flow leading to the intake, the velocity within the flow area, the critical submergence level, and the dimensions of the intake itself [6].

Reduced scale experimental tests have become the preferred method of evaluating pump intake designs concerning the criteria specified by ANSI/HI 9.8-2012 in recent years. Nonetheless, these tests come with several limitations, including substantial expenses, extended timeframes for constructing testing facilities, and restricted availability of skilled testing professionals. In contrast, Computational Fluid Dynamics (CFD) analysis offers the advantage of delivering more comprehensive insights into the flow field, all while being considerably more cost-effective and quicker than experimental tests using scale models.

Constantinescu and Patel carried out three-dimensional numerical simulations to examine the flow dynamics within a rectangular pump intake [7]. They utilized a range of turbulence models to accurately represent the critical flow features around the pipe intake in both symmetric and asymmetric configurations. Ansar and Nakato conducted experimental investigations on three-dimensional flows in pump intakes [8]. Hwang and Yang evaluated the efficiency of pumps by employing various flow-straightening devices through experimental approaches [9]. Li et al. conducted RANS simulations to examine the distribution of streamwise velocity, contrasting their findings with data collected from the upstream channel and above the pump throat [10]. Tokyay and Constantinescu assessed the accuracy of large eddy simulation (LES) and RANS models by comparing their predictions with measurements obtained via particle image velocimetry [11]. Issa and Bayeul-Lainé used FLUENT software to predict the 3D flow field in a rectangular pump basin [12]. Chuang et al. conducted both experimental and numerical investigations to explore the effects of sluice gate submergence and discharge on flows in pump basins [13]. Their findings reveal that discharge and

gate submergence have an inverse connection with efficiency of the pump. Kim et al. investigated the effectiveness of rectangular and trident-shaped bars as anti-vortex devices (AVDs) positioned at the bottom of the pump intake channel, just below the bell-mouth [14]. Their study revealed that placing the AVDs at the site of vortex formation eliminates the vortex and promotes a more uniform flow. The majority of past CFD research on pump intake systems has concentrated on modelling the intricate and turbulent flow patterns near the suction pipe of a solitary sump, as well as assessing the effectiveness of various anti-vortex devices [15-17]. The focus on the comprehensive modelling of the entire system, which encompasses the supply lines, screens, sumps, forebay, and pump pipes, is not given as much consideration. Choi et al. conducted a study using both experimental tests and numerical modelling to examine the consistency of flow in a model of a pump sump with multiple intakes [18]. The findings indicated that it is crucial to thoroughly analyse the flow patterns in the forebay diffusing area at the upstream section of the pump intake inlet.

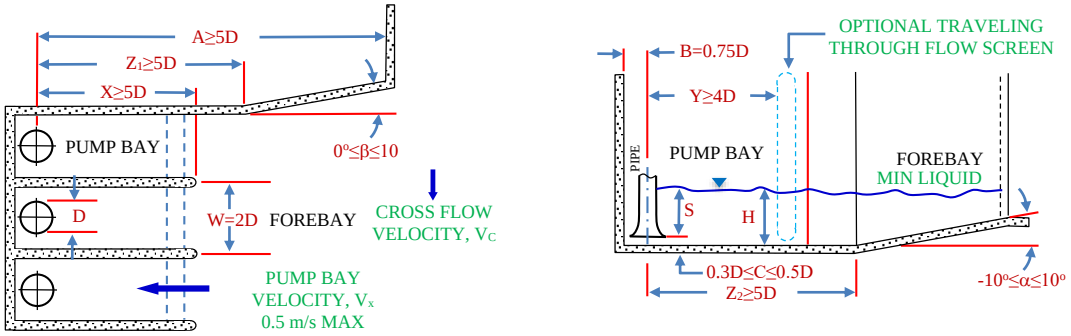

Fig. 1: Recommended intake structure layout by ANSI/HI 9.8-2012

Using a hydraulic model of the seawater intake system at the Aliveri Power Plant in Greece, this study investigates the impact of cross-flow velocity in the forebay on the swirl angle within the pump suction pipes [19]. The experimental tests revealed that a significantly non-uniform velocity profile emerges in the forebay when one of the two cleaning channels is closed. Nasr et al. performed numerical simulation of the turbulent flow in a multi-unit pumping station using Ansys-CFX [20]. The research concluded that the flow pattern in the forebay of the lateral inlet pumping station can be significantly enhanced by implementing a parabolic wall along with several rectification piers. Longo et al. addressed some of the key questions regarding the applicability of CFD modelling using OpenFOAM for assessing the hydraulic performance of pumping installations [21]. Zhang et al. examined how the flow pattern in a forebay with a side intake pumping station can be enhanced through the use of diversion piers [22]. They used the FLUENT software for CFD analysis and reported that the diversion piers had a significant adjustment of uniformity of axial flow velocity and weighted average angle of flow velocity. Yamini et al. reported results of a three dimensional CFD modelling using FLOW-3D software for the performance evaluation of a seawater intake system [23]. The results suggest that designers should take all possible measures to eliminate small entrances and filtration areas leading from the basin to the bottom of the intake forebay.

The uniqueness of this study is found in its flow analysis objectives, which aim to simulate the entire seawater intake system while also exploring various operating scenarios for both the system and pump stations. Additionally, the study investigates the impact of guide vanes on enhancing the flow pattern in the forebay area and the approach flow to the pump bays under both symmetric and asymmetric operating modes.

The paper is organized into five distinct sections to provide a comprehensive overview of the research. The first section covers the methodology, detailing the approaches and techniques used in the study. Following that, the second section focuses on the validation of the numerical simulation, ensuring the accuracy and reliability of the results obtained. The third section describes the study area, outlining the geographical and environmental context of the research. Next, the fourth section presents the numerical model setup, explaining the configuration and parameters used in the simulations. Finally, the fifth section discusses the results and analysis, interpreting the findings and their implications in relation to the study objectives.

2. Methodology

In this study, the three-dimensional Reynolds-Averaged Navier-Stokes (RANS) equations for incompressible water flow are employed for numerical simulations. The continuity equation, along with the Reynolds-averaged momentum equations in Cartesian coordinates ($x_i, i = 1,2,3$), can be represented as follows [24]:

$$\frac{\partial \overline{u_\iota}}{\partial x_i} = 0 \tag{3}$$

$$\rho \overline{u_j}\frac{\partial \overline{u_\iota}}{\partial x_j} = \rho g_i + \frac{\partial}{\partial x_j}\left[-\bar{p}\delta_{ij} + \mu\left(\frac{\partial \overline{u_\iota}}{\partial x_j} + \frac{\partial \overline{u_j}}{\partial x_i}\right) - \rho\overline{u_\iota' u_j'}\right] \tag{4}$$

Here, $\overline{u_\iota}$ is the time averaged velocity component, $\bar{p}$ is the mean pressure, g_i is the gravity acceleration, ρ and μ are the density and dynamic viscosity of water, respectively. δ_{ij} is the Kronecker delta and $-\rho\overline{u_\iota' u_j'}$ is the Reynold stress tensor, where $i, j = 1,2,3$.

There are various models available to estimate Reynolds stresses, but none of them are universally accepted to solve the diverse range of problems encountered in turbulent flows [25]. In this study, the Reynolds Stress Model (RSM) is utilized due to the significant strain rates in fluid elements and the presence of circulation and separation zones across various flow areas in the forebay and intake channels. The Reynolds Stress Model tackles the RANS equations by solving seven transport equations associated with Reynolds stresses, in addition to an extra equation for the dissipation rate of turbulent kinetic energy (ε). As highlighted by Launder, the Reynolds Stress Model (RSM) is more adept at capturing the effects of streamline curvature, vorticity, circulation, and rapid changes in strain rate compared to two-equation models [26]. However, it requires significantly more computational resources and time. The transport equation for this model can be expressed as Equation (5), as stated by Launder [26]. The left-hand side terms are the local time derivatives and convection term, C_{ij}, respectively, while the right-hand side terms are the turbulent diffusion, $D_{T,ij}$, molecular diffusion, $D_{L,ij}$, stress production, P_{ij}, pressure-strain, ϕ_{ij}, dissipation rate, ε_{ij}, and production by system rotation, F_{ij}, respectively.

Linear or quadratic models can be utilized to compute the pressure-strain term. The complete closure of the Reynolds-averaged momentum equation is achieved by employing the individual Reynolds stresses. Numerical simulations were performed using *ANSYS FLUENT* software. It solves the governing equations using finite volume method (F.V.M) in conjunction with different turbulence models. The governing equations are integrated over each control volume to formulate discretized algebraic equations for the dependent variables.

$$\underbrace{\frac{\partial \rho\overline{u_\iota' u_j'}}{\partial t}}_{local\ time\ derivatives} + \underbrace{\frac{\partial}{\partial x_k}\left(\rho\overline{u_k}\,\overline{u_\iota' u_j'}\right)}_{C_{ij}} = \underbrace{-\frac{\partial}{\partial x_k}\left[\left(\rho\,\overline{u_\iota' u_j'}\,u_k'\right) + \overline{p'\left(\delta_{kj}u_\iota' + \delta_{\iota k}u_j'\right)}\right]}_{D_{T,ij}}$$
$$\underbrace{+\frac{\partial}{\partial x_k}\left[\mu\frac{\partial}{\partial x_k}\left(\overline{u_\iota' u_j'}\right)\right]}_{D_{L,ij}} \underbrace{-\rho\left[\left(\overline{u_\iota' u_j'}\frac{\partial \overline{u_j}}{\partial x_k} + \overline{u_j' u_k'}\frac{\partial \overline{u_\iota}}{\partial x_k}\right)\right]}_{P_{ij}}$$
$$\underbrace{+p'\overline{\left(\frac{\partial u_\iota'}{\partial x_j} + \frac{\partial u_j'}{\partial x_\iota}\right)}}_{\phi_{ij}} \underbrace{-2\mu\left(\frac{\partial u_i'}{\partial x_k}\frac{\partial u_j'}{\partial x_k}\right)}_{\varepsilon_{ij}}$$
$$\underbrace{-2\rho\Omega_k\left(\overline{u_j' u_m'}\varepsilon_{ikm} + \overline{u_\iota' u_m'}\varepsilon_{jkm}\right)}_{F_{ij}} \tag{5}$$

To discretize the convection terms of the transport equations, second order Upwind (SOU) scheme has been utilized. Since the governing equations are coupled and nonlinear, iterations are necessary to attain a converged solution. Therefore, the coupling of velocity and pressure has been carried out through the SIMPLE algorithm. Gambit software was used to create the geometry, generate the computational grid and assign appropriate boundary conditions for various surfaces.

3. Validation of Numerical Simulation

To evaluate the capability of the CFD model, a benchmark case is selected which consists of a single pump with a circular pipe in a rectangular intake channel, as illustrated in Figure (2-a). The selected basin geometry mirrors the model created by Constantinescu and Patel and adheres to the dimensions and flow conditions outlined in the ANSI/HI 9.8-2012 guidelines [7]. The inset of the figure provides a summary of the geometric and hydraulic characteristics of the benchmark model. Figure (2-b) shows 3D and 2D views of the computational meshes. In order to discretize the computational domain, non-uniform curvilinear meshes are utilized. The grid lines are stretched around the pipe and at the pump pipe inlet level to ensure an accurate simulation of the subsurface and surface vortices. In addition, the computational meshes are refined in the near vicinity of the side walls, back wall, and channel bed. This is done to ensure that the non-dimensional distance from the wall to the first node is set to $Y^+ or\ Z^+$=5. A total of 520,000 computational cells are utilized to discretize the computational domain. Figure 2(c) shows the implemented boundary conditions at various surfaces. At the inlet of the channel 'VELOCITY INLET' boundary condition is imposed with uniform velocity U_{in} = 0.065m/s. Values of inlet turbulence kinetic energy (k) and its dissipation rate (ε) are computed using equations presented in the manual of the FLUENT, by assuming the turbulence intensity, $T.I$ =2%. For the side walls, channel bed, and pump pipe, 'WALL' boundary condition is used and all walls have been assumed smooth. Standard wall function is used to bridge the inner region between the wall and the turbulence fully developed region. Symmetry boundary condition have been implemented to the top surface of the channel. At the outlet of the pipe,

'VELOCITY INLET' boundary condition is used with vertical upward velocity, U_p= 0.6m/s. Zero velocity has been assumed in all of the computational cells as the initial value and, to assess the convergence of iterations for different governing equations, the scaled residual for each conserved variable was computed and monitored during numerical solution. In addition, flow variables at different points, the general flow field in various planes, and mass inflow and outflow were monitored during the simulation to ensure convergence of the numerical solution. Convergence was achieved with a residual level of 10-6 and 550 iterations. Figure (3) presents a comparison between the calculated and measured streamwise velocities at the $y/h = 0.2$ plane across various sections of the approaching channel. The streamwise velocity, denoted as U, is normalized by the bulk velocity U_p= 0.6m/s within the pump column. The data indicates a satisfactory agreement between the calculated results and the experimental measurements. The root mean square error (RMSE) between the calculated and measured velocity profiles is quantified as 0.004.

Figure (4) compares the 2D streamlines between the results of the present study and the results reported by Constantinescu and Patel [7]. Flow patterns in different surfaces has a very good compliance with the results presented in the literature, and the rotating flows in different parts of the field have been predicted accurately. According to Figures (3-a) and (4-b) approaching horizontal flow at the upstream of the pipe is diverted to the sides of the pipe and after separating from the pipe's outer wall, two symmetrical vortices (V2) formed, behind the pipe. This vortex is a type of surface vortices and by moving from the upper layers towards the bed of the channel, while reducing the dimensions of the vortex, its core is drawn towards the pipe inlet. Corner surface vortices (V1) formed at the junction of the side walls and the channel back wall. Figure (4-c) shows that in the middle vertical plane of the channel a downward flow forms behind the pipe and the upper layer flow is drawn into the pipe in a helical manner. Two separation zones formed inside the pipe, with one at the upstream part being more extended. The majority of streamlines entering the suction pipe are concentrated at the upstream part, and the oblique upward flow that bounds the separation zones aligns with the pipe when the upward pipe suction overcomes the longitudinal momentum of the channel flow. Figure (4-d) shows clear evidence of the formation of a vortical flow with a horizontal axis of rotation. Flow visualization at different vertical planes indicates that this vortex extends in both longitudinal and vertical directions as one moves from the side walls towards the symmetry plane of the channel.

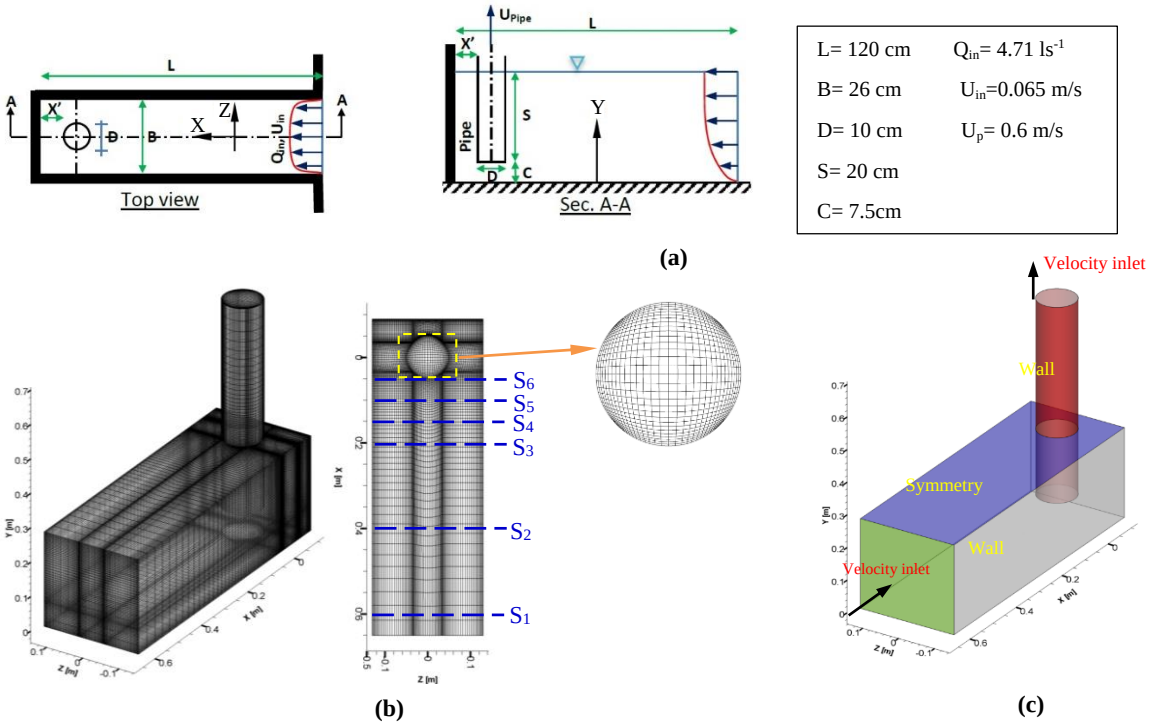

Fig. 2: The benchmark model of the single pump intake in a rectangular channel; (a) geometric and hydraulic characteristics, (b) computational mesh in 3D and 2D views and (c) implemented boundary conditions

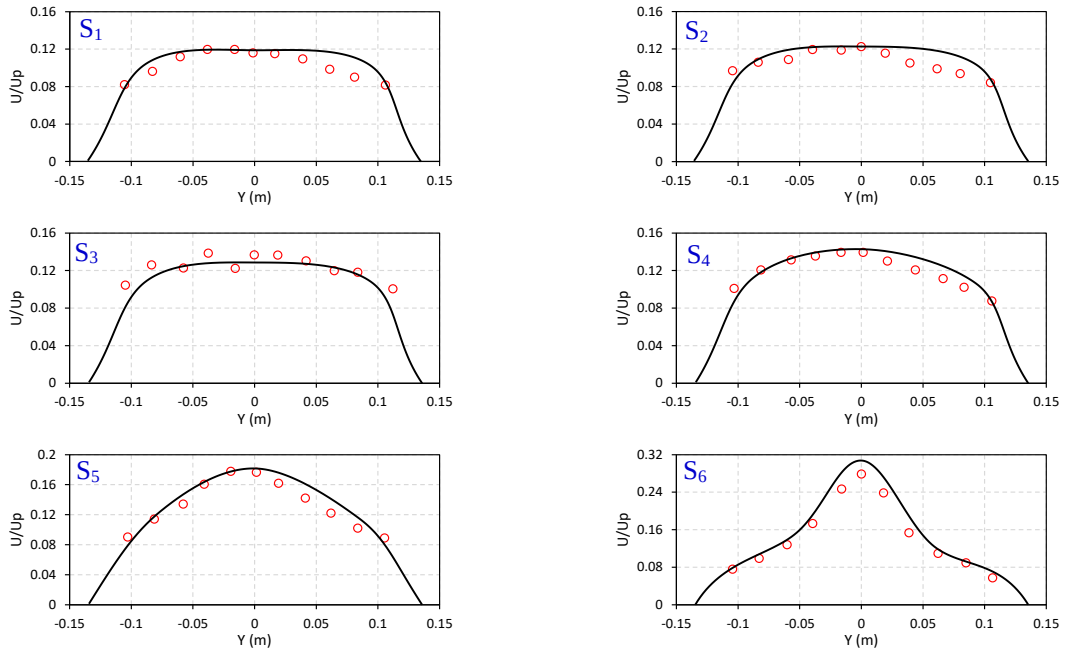

Fig. 3: Comparison of the stream wise velocity profiles between results of the present study (black line) and experimental measurements (red circles) at the $y/h = 0.2$ plane across various sections of the approaching channel

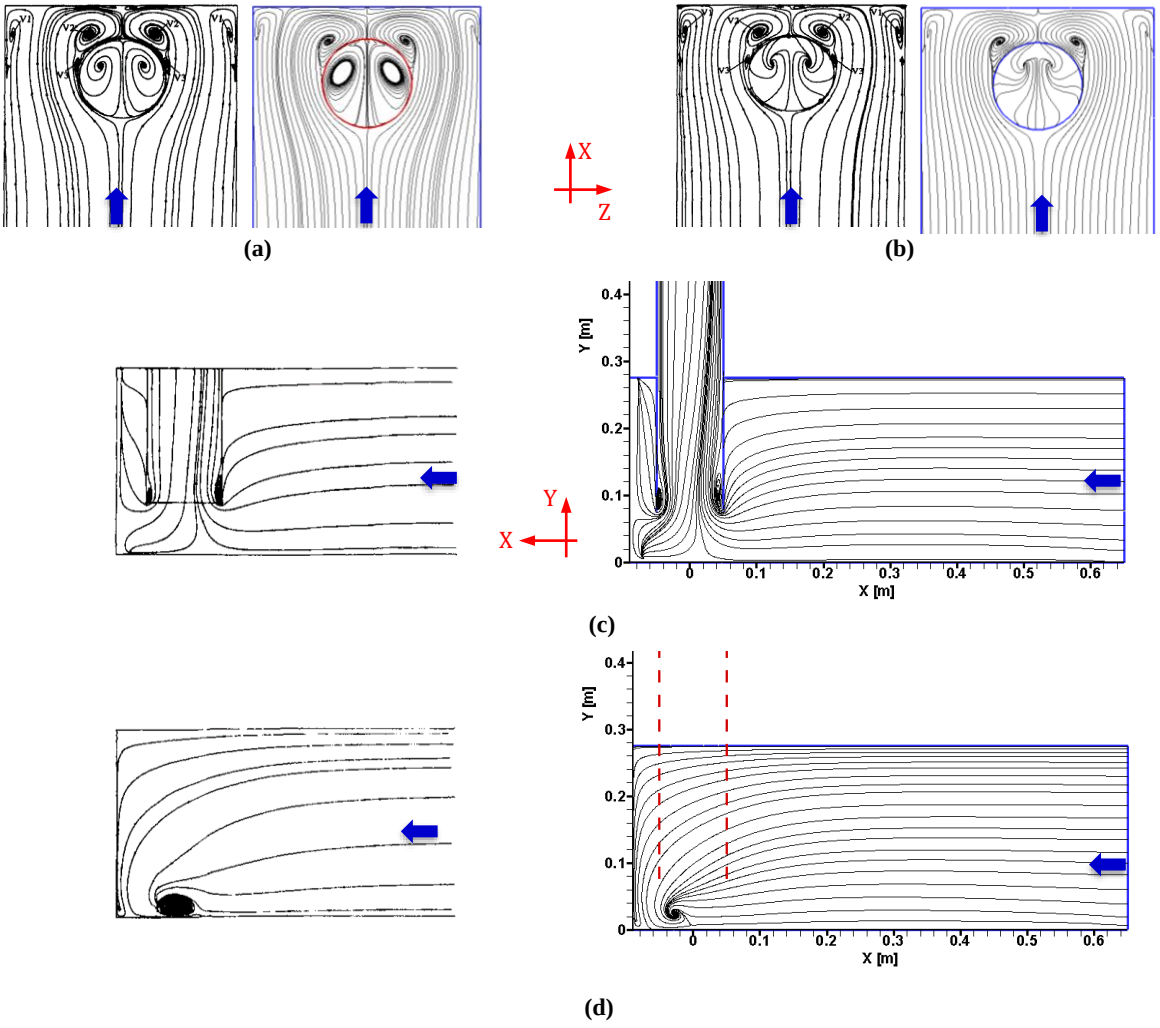

Fig. 4: Comparison of the 2D streamlines between results of the present study (right) and results presented by Constantinescu and Patel, 1998 (left); (a) XZ plane @ Y=2.75D, (b) XZ plane @ Y=1.75D, (c) XY plane @ basin symmetry plane, and (d) XY plane @ 0.5D from the side wall

The results presented in this section confirms the capability of the CFD software used for simulating 3D complex flow in the pump intake channel. Additionally, the correct choice of boundary conditions is confirmed based on the obtained accurate results. In the following section, the study area is introduced, and the results of CFD analysis are presented for an integral seawater pump intake system.

4. Study Area and Case

Figure (5) illustrates the study area. Bandar Abbas desalination plant, at the shore of the Persian Gulf in Iran, is situated in the west of the Bandar Abbas port city, between the Persian Gulf Star Oil Company (PGSOC) Basin and the Persian Gulf Port. The foreseen capacity of potable water production is 100,000 m^3/day, for which 330,000 m^3/day of salty water should be delivered to the process units. The initial geometry of the seawater intake system which has been designed based on ANSI/HI 9.8-2012 standard is illustrated in Figure (6).

Seawater is delivered to the basin using two inlet pipes with a diameter of 1500 mm. The water entering the basin is divided into two parts using two channels with a width of 4000 mm, equipped with stop logs and coarse and fine screens.

The transition angle of the common inlet part of the basin is 29 degrees. The forebay has diverging side walls with an angle of 44 degrees and a maximum width of 25400 mm. Nine rectangular pump bays are considered to deliver the seawater to the desalination plant. The width of each bay is 2200 mm. The diameter of the pump pipe is 1100 mm, and two pumps, the first and last, are considered for the future development plan. Some detailed geometric specifications of the pump basin are summarized in the inset of Figure (6). Geometric variables were previously defined in Figure (1).

5. Numerical Model Setup

Figure (7-a) shows the 3D geometry of the seawater intake system and the boundary conditions used at various surfaces of the computational domain. Pumps are numbered from right to left. As it depicted in this figure at the inlet pipes, the "INLET VELOCITY" boundary condition is used and the (inlet discharge per pipe) / (pipe area) is used as the water velocity entering the basin. All of the solid boundaries are considered as "WALL" boundaries.

At the top boundary of the pump pipes, the "INLET VELOCITY" boundary condition is used and the W-velocity component with corresponding value according to the detailed operating scenario, which will be presented later, has been imposed to the outlet boundary of each pipe. Coarse and fine filters are modelled as porous media with 80% and 50% porosity, respectively.

Minimum sea water level is used as the critical hydraulic condition in the basin. Minimum water level in the basin is -2.80 m and as it depicted in Figure (6b) the basin bed level is -5.8 m. The upper vertical boundary is placed at level -2.8 m and the "SYMMETRY" boundary condition is imposed to the top boundary of the basin.

The error resulting from neglecting water surface variations is minimal when the maximum water surface elevation remains below 10% of the total basin depth [27]. Figures (7b) and (7c) show computational meshes in three dimensional and two-dimensional views, respectively. Triangular cells with various mesh sizes are used to discretize the computational domain. The total number of cells is 1,606,166. Similar to the benchmark case, zero velocity has been assumed in all of the computational cells as the initial value.

Scaled residuals of the governing equations, flow variables and mass inflows and outflows are monitored during iterations to ensure the convergence of the numerical solutions. In all cases, convergence was achieved with the residual level of 10^{-6} and the number of iterations of 3700.

Two different operating modes are considered for the basin:

(1) Both of the channels are in operation and the total inlet discharge from two inlet pipes is 330000 m^3/day (Symmetric operation mode).

(2) For maintenance and repair purposes, the left channel (channel 2) is considered closed and discharge of the inlet pipes is 70% of the total discharge, 231000 m^3/day (Asymmetric operation mode).

Different operating scenarios for pump intakes are considered for each operation mode of the basin, as presented in Tables (1) and (2). In total, ten models are run to analyze the hydrodynamics of the basin in the initial design condition.

Based on the results of this analysis, a modified geometry is presented to improve the flow pattern of the basin. The hydrodynamic performance of the seawater intake system will then be compared between the initial design and modified conditions.

Fig. 5: Location of the Bandar Abbas seawater desalination plant, Hormozgan province, Iran

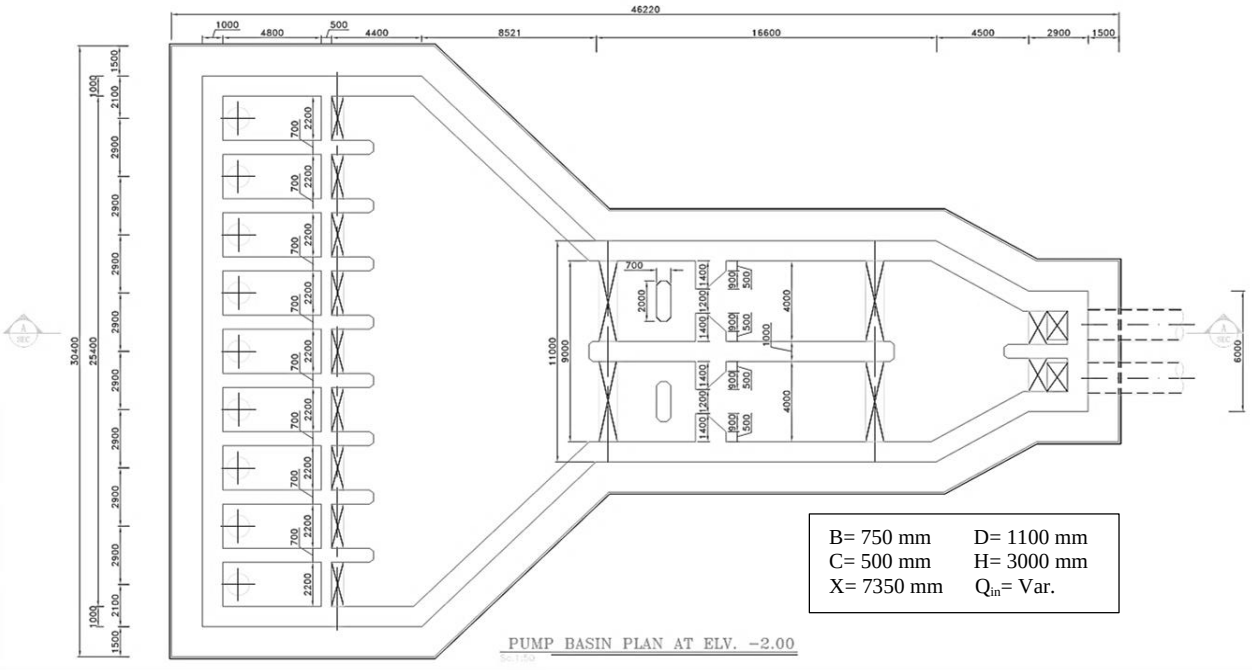

(a)

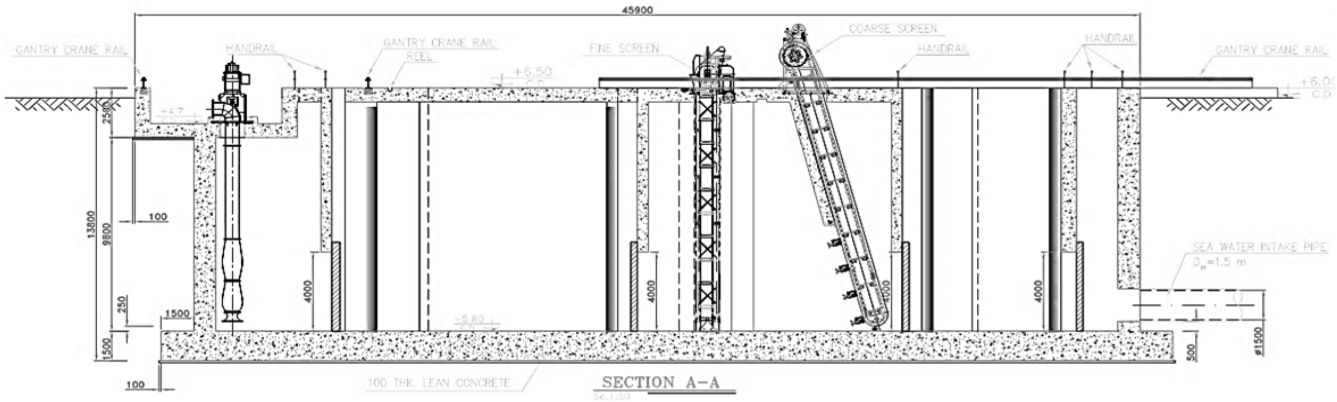

(b)

Fig. 6: General layout of the Bandar Abbas seawater intake system; (a) top view, and (b) side view, section A-A.

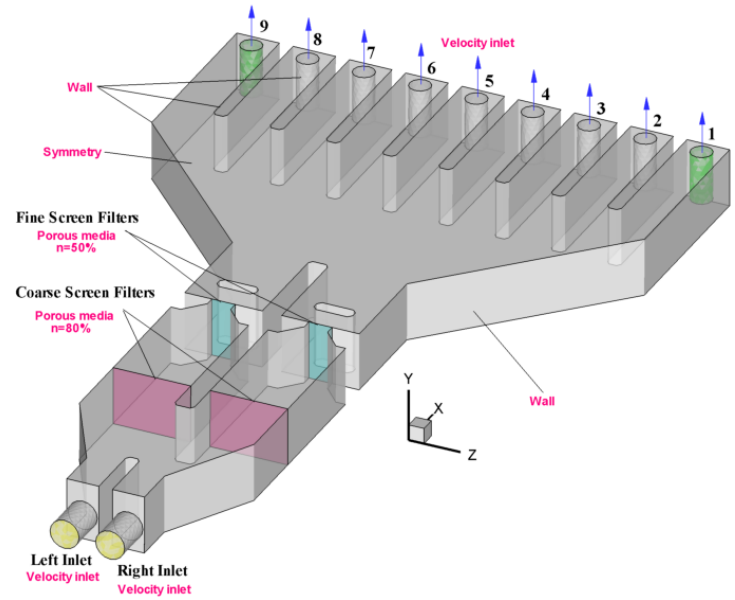

(a)

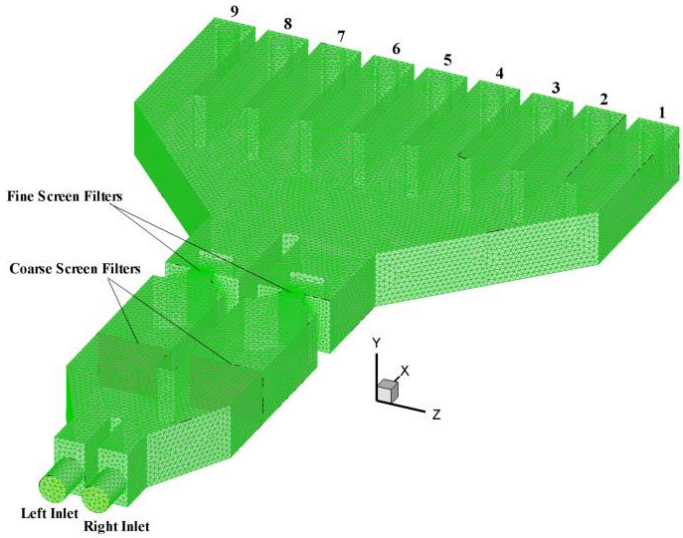

(b)

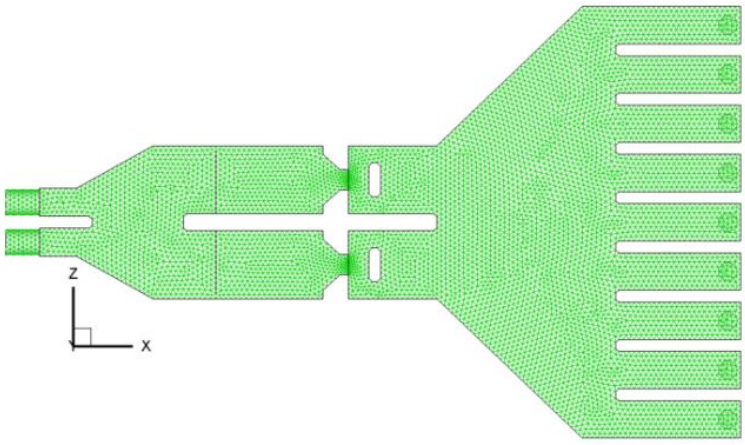

(c)

Fig. 7: CFD model setup of the Bandar Abbas seawater intake system; (a) 3D geometry and boundary conditions, (b) 3D view of the computational cells, and (c) 2D view of the computational cells at pump pipes inlet level (Y=-5.3 m)

6. Results and Analysis

6.1 Hydrodynamics of the Initial Geometry

Figure (8) shows the results of the CFD analysis for the Sym-1 operating scenario. According to Figsures (8-a) and (8-b), at the downstream end of the left and right channels, the flow hits the vertical walls, and four jet-like flows form at the inlet of the forebay. The middle jets on both sides of the symmetry line result in a straight high-velocity flow to the pump intake #5, while the side jets, after interacting with the low-velocity flow in the forebay, result in strong transverse flows parallel to the diverging side walls of the forebay.

Figures (8-c) and (8-d) show the 2D flow pattern in Y= -2.7 m plane and 3D streamlines in the whole domain, respectively. The 2D velocity field shows that due to the significant momentum transfer between the high-velocity side jet flows and low-velocity flow in the forebay, two dead zones form on both sides of the forebay. The dead zones extend to the inlet of the pump bays and cause strong transverse flows. As a result, recirculating zones form along pump bays #3, 4, 6, and 7. The depth-varying structure of the dead zones is clearly illustrated using 3D streamlines.

Figure (9) compares the depth-averaged velocity vectors for different operating scenarios of the pump intakes in the symmetric operation mode of the basin. Due to the formation of dead zones in the forebay area, in all scenarios, non-uniform flow forms at the inlet of the pump bays, except for pump bay #3 in the operating scenario Sym-4.

Table 1: Operating scenarios of the pump intakes in the symmetric operation mode of the basin

Scenario code Discharge	Pump1*	Pump2	Pump3	Pump4	Pump5	Pump6	Pump7	Pump8	Pump9*
Sym-1	Off	Off	On	On	On	On	On	Off	Off
Q (m^3/s)	0	0	0.764	0.764	0.764	0.764	0.764	0	0
Sym-2	Off	Off	Off	On	On	On	On	On	Off
Q	0	0	0	0.764	0.764	0.764	0.764	0.764	0
Sym-3	Off	On	On	On	Off	Off	On	On	Off
Q	0	0.764	0.764	0.764	0	0	0.764	0.764	0
Sym-4	Off	Off	On	Off	On	On	On	On	Off
Q	0	0	0.764	0	0.764	0.764	0.764	0.764	0
Sym-5	Off	On	Off	Off	On	On	On	On	Off
Q	0	0.764	0	0	0.764	0.764	0.764	0.764	0

* Pumps1 and 2 are considered for the future development plan. Q is discharge.

Table 2: Operating scenarios of the pump intakes in the asymmetric operation mode of the basin.

Scenario code Discharge	Pump1	Pump2	Pump3	Pump4	Pump5	Pump6	Pump7	Pump8	Pump9
Asym-1	Off	On	On	On	On	Off	Off	Off	Off
Q (m^3/s)	0	0.668	0.668	0.668	0.668	0	0	0	0
Asym-2	Off	Off	On	On	On	On	Off	Off	Off
Q	0	0	0.668	0.668	0.668	0.668	0	0	0
Asym-3	Off	On	Off	On	On	On	Off	Off	Off
Q	0	0.668	0	0.668	0.668	0.668	0	0	0
Asym-4	Off	On	On	Off	Off	On	On	Off	Off
Q	0	0.668	0.668	0	0	0.668	0.668	0	0
Asym-5	Off	On	Off	On	Off	On	Off	On	Off
Q	0	0.668	0	0.668	0	0.668	0	0.668	0

Figure (10) presents the results of the CFD analysis for the Asym-1 operating scenario. The velocity magnitude distribution in the near-bed and near-water surface planes indicates that high-velocity jet flows are redirected towards the right side of the forebay. This behavior is attributed to the development of a significant dead zone on the left side of the forebay. Additionally, all four operational pumps are situated on the right side of the intake system, causing the inflow to the forebay to be directed toward the intakes of these pump bays.

Figures (10c) and (10d) illustrate the establishment of a substantial dead zone on the left side of the forebay, alongside a smaller dead zone forming along the right wall. The interaction between these dead zones and the jet flows generates pronounced transverse flows at the inlets of pump bays #2 and #3. The resulting non-uniform oblique inlet flow has led to the emergence of separation zones along these channels. Figure (11) displays the depth-averaged velocity vectors for various operating scenarios of the pump intakes under the asymmetric operation mode of the basin. In this operational mode, unfavorable flow conditions in the forebay give rise to non-uniform flow patterns along the pump bays.

6.1.1 Compliance with ANSI/HI 9.8-2012 Standard Performance Criteria

To quantitatively assess the uniformity of the incoming flow at each pump bay, the flow uniformity index (U.I.) is utilized for the flow velocity in the pump intake channels. This index is derived from the concept of standard deviation, as shown in Eq. (6):

$$U.I. = \sqrt{\frac{\int_{z=0}^{z=B} (u(z) - \bar{u})^2 \, dz}{B}} \Big/ \bar{u} * 100 \quad (6)$$

In this context, $u(z)$ represents the local depth-averaged velocity, while $\bar{u}$ refers to the average velocity across the inlet of the pump intake channel.

Figure (12-a) displays the calculated flow uniformity index for the incoming flow at the pump intakes, comparing both symmetric and asymmetric operating modes of the Bandar Abbas seawater intake system.

Among the average flow uniformity values in the pump intake channels, the Asym-5 scenario exhibits the highest index at 130%. This indicates the greatest standard deviation of local velocity relative to the average velocity on the y-z cross-sectional plane of the intake channel. The figure demonstrates that the asymmetric operation of the intake system results in more unfavorable flow conditions in the forebay area, leading to increased flow non-uniformity along the pump bays compared to the symmetric mode. In the symmetric operating mode, the Sym-3 scenario recorded the highest uniformity index of 110%.

The swirl angle in the pump pipes was determined using Equation (2), and the average swirl angles across all pumps for different operational scenarios are presented in Figure (12b). This figure indicates that, in all scenarios, the average swirl angle exceeds the maximum allowable value of 7° as recommended by the ANSI/HI 9.8-2012 standard. The highest average swirl angles were observed in the Sym-3 and Asym-5 scenarios for the symmetric and asymmetric operating modes, respectively. The maximum inlet bell velocity across ten different operating scenarios was measured at 0.72 m/s, which is below the 2.4 m/s threshold recommended by the ANSI/HI 9.8-2012 standard.

As shown in Figures 9 and 11, robust transverse flows develop at several pump bay inlets due to the presence of circulating zones in the forebay. In some instances, the cross-flow velocity ((V_c)) exceeds 50% of the inlet velocity at the pump bays.

The CFD analysis results for the initial design geometry of the Bandar Abbas seawater intake system reveal the formation of multiple unfavorable dead zones and circulating zones along the forebay. The intricate flow structures in this region contribute to non-uniform flow and the emergence of separation zones along the pump bays. Furthermore, the considerable diverging angle in the forebay's diffusing zone may create unstable and fluctuating flow conditions at the pump intake channels. To mitigate these issues, geometric modifications have been proposed, with the results of the CFD analysis for the modified geometry detailed in the subsequent section.

6.2 Hydrodynamics of the Modified Geometry

This section investigates the influence of guide vanes on the modification of the flow field in the forebay area of the Bandar Abbas seawater intake system. This analysis is crucial, as understanding how the hydraulic modifications affect flow dynamics can lead to enhanced performance of the seawater intake process.

Figure (13-a) presents a three-dimensional representation of the intake system, which includes the installation of three guide vanes at the forebay inlet. Figure (13-b) provides detailed dimensions and specification regarding the design of the guide vanes.

Each guide vane has a specified length of 4700 mm, and the two side vanes are positioned at an angle of 22° relative to the centerline of the basin. This angled installation is designed to optimize flow direction and enhance overall flow dynamics. Additionally, triangular noses, each measuring 350 mm in length, are affixed to both ends of the vanes to prevent flow separation at the upstream and downstream locations.

By mitigating flow separation, these design features aim to improve the stability and efficiency of the flow entering the intake channels. Figure (13-c) illustrates the computational

meshes used to model the modified basin geometry. Notably, there is a refined density of computational cells specifically in the forebay area, resulting in a total of 1,801,254 cells. This high spatial resolution in the mesh allows for a detailed representation of complex flow interactions, which is essential for accurately predicting hydraulic performance.

Comprehensive Computational Fluid Dynamics analyses have been performed to assess the performance of the guide vanes within the modified basin geometry under both the Sym-3 and Asym-5 operating scenarios. During the simulations, a "WALL" boundary condition has been applied to all surfaces of the guide vanes to emulate the effect of the physical structure on the flow without allowing any flow penetration through the boundaries. The remaining boundary conditions have been maintained in accordance with those employed in the initial model to ensure comparability and validity of the results.

Figure (14) compares the flow field characteristics of both the initial and modified basin designs during the Sym-3 operational scenario. The implementation of guide vanes in the modified geometry effectively redistributes the inlet flow towards the forebay, directing the flow radially into the intake channels.

This configuration eliminates the presence of dead or circulating flow zones in the forebay, while minimizing cross-flow into the pump bays. The enhanced flow configuration also indicates that there are no separation zones along the intake channels, significantly contributing to a uniformly distributed approach flow to all pump pipes.

Further analysis is presented in Figure (15), which displays contour plots of velocity magnitude at cross-sections near the pump pipes for the modified geometry in the Sym-3 scenario.

The results confirm that the flow approaching the pumps maintains uniformity across the entire depth of the channels. This uniform flow pattern is vital in preventing localized high-velocity regions that could potentially lead to increased wear and tear on the pump components.

In the Asym-5 scenario, a detailed comparison is provided in Figure (16), showcasing the distribution of velocity magnitude, depth-averaged velocity vectors, and the two-dimensional flow field for both the initial and modified basins.

The analysis reveals that in the initial basin configuration, high-velocity jets originating from the right channel are redirected to the left side of the forebay. This redirection leads to the formation of a significant circulating zone that occupies nearly the entire left half of the forebay and introduces adverse flow conditions across the system. Accompanying this, a recirculating flow zone establishes along the right wall of the forebay, exacerbating the issue and generating pronounced transverse flows at the inlets of the pump intake channels.

Moreover, the presence of extensive separation zones along channels #2, 6, and 8 results in completely non-uniform pump approach flow in these regions. These unfavorable flow characteristics highlight the importance of geometry modifications in improving operational efficiency. The differences between the flow patterns of the initial and modified geometries are stark; in the modified geometry, the high-velocity jet flows effectively dissipate upon interaction with the guide vanes, which assists in aligning the inlet flows of the pump forebays with the channels. Consequently, all operating pumps experience a uniformly distributed approach flow, which is a critical factor for their performance and longevity.

Figure (17) further depicts the velocity magnitude contour plots at cross-sections near the pump pipes in the Asym-5 scenario. The findings indicate that, with the exception of pump #6—which experiences a slightly non-uniform approach flow—all other pumps receive a completely uniform flow throughout the entire depth of their respective channels. Notably, the non-uniformity of the approach flow to pump #6 in the modified basin geometry is significantly less pronounced than the flow non-uniformity observed in the initial configuration. This reduction in flow non-uniformity for pump #6 underscores the effectiveness of the guide vanes in optimizing hydraulic conditions.

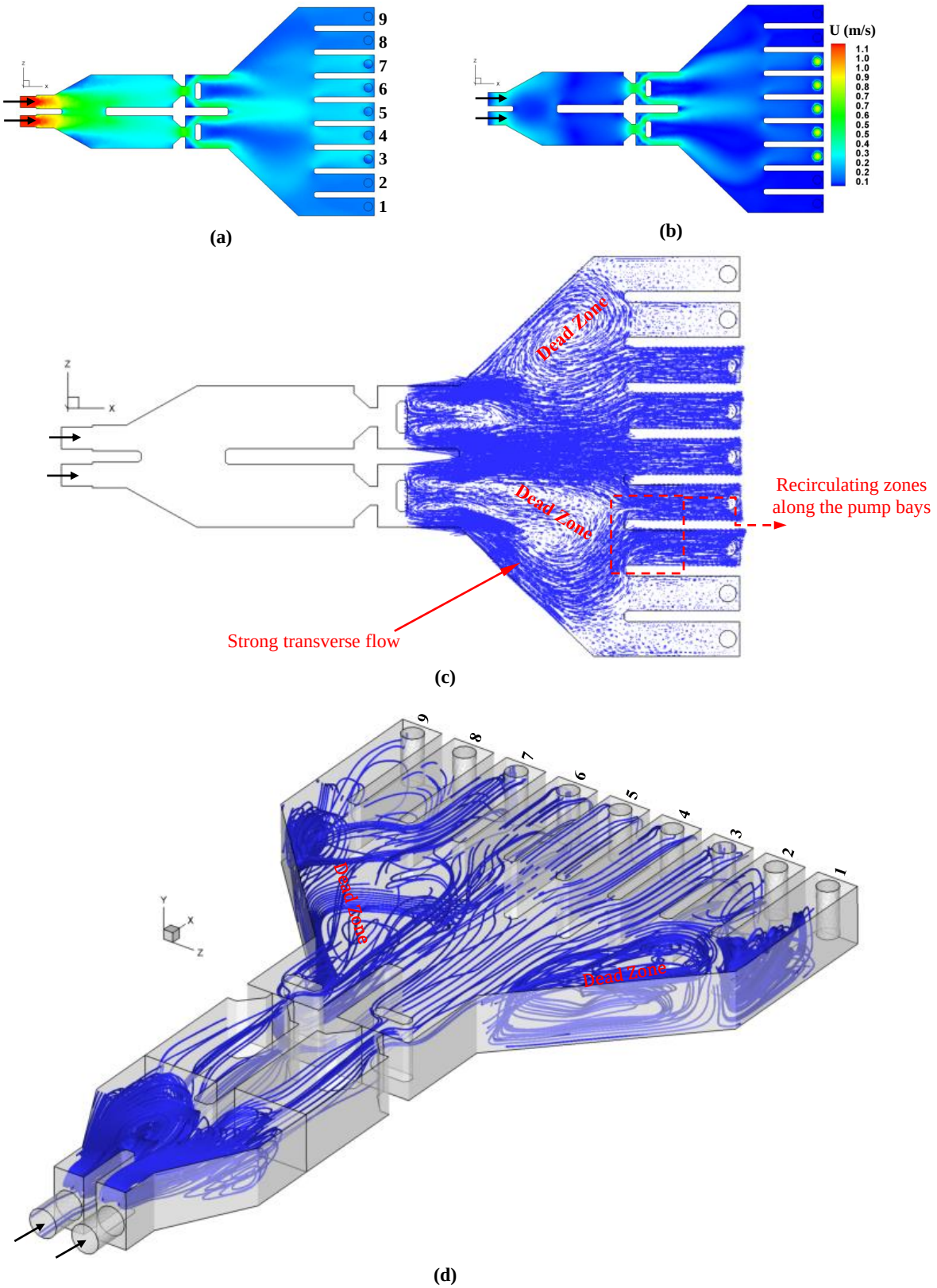

Fig. 8: Results of CFD analysis for Sym-1 scenario; (a) distribution of the velocity magnitude in Y= -5.7 *m* plane, (b) distribution of the velocity magnitude in Y= -2.7 *m* plane, (c) flow pattern in Y= -2.7 *m* plane, and (d) three dimensional streamlines

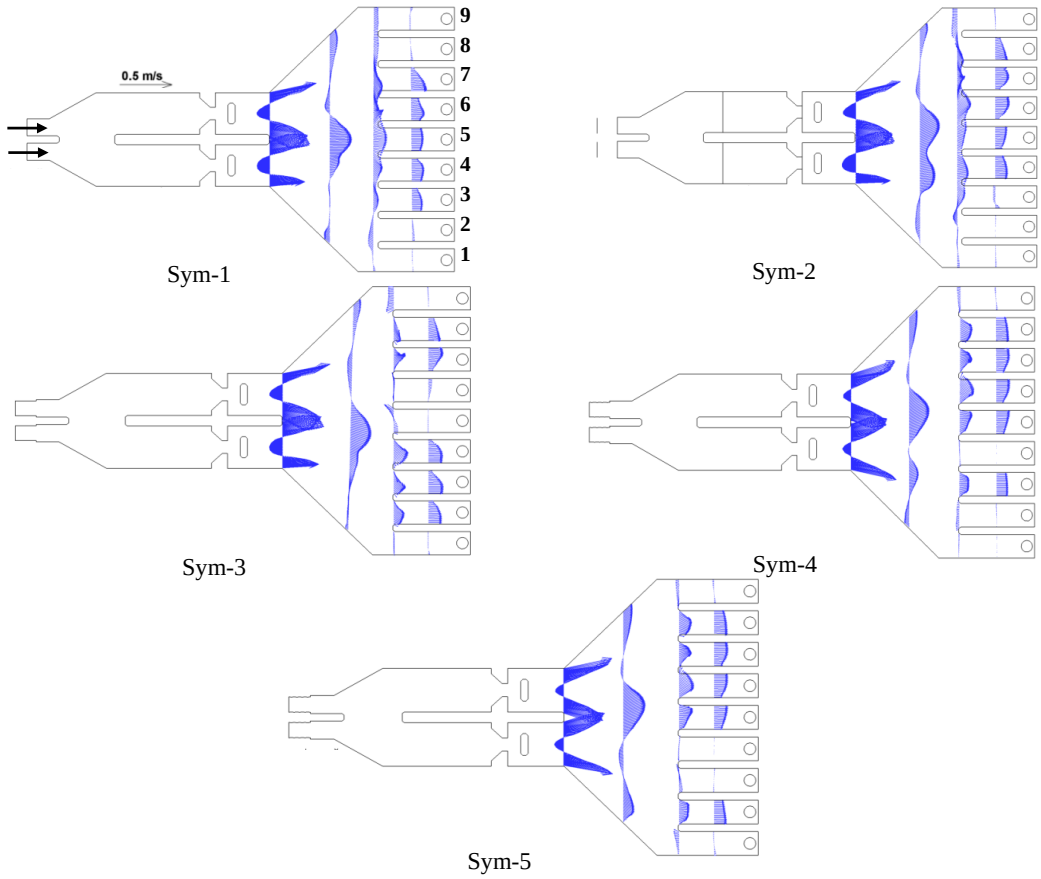

Fig. 9: Depth-averaged velocity vectors for different operating scenarios of the pump intakes in the symmetric operation mode of the basin.

In the modified basin geometry, the assessment of the average flow uniformity index (U.I.) revealed notable results regarding the incoming flow conditions at the pump intakes. Specifically, the U.I. values for the Sym-3 and Asym-5 operational scenarios were determined to be 24% and 27%, respectively. These findings indicate a marked enhancement in flow uniformity compared to the initial basin configuration, which exhibited significantly lower indices. Improving the uniformity index (U.I.) is critical for the optimal performance of pump systems, as it indicates a more consistent and stable flow profile.

A higher U.I. reflects a uniform flow entering the pumps, which plays a crucial role in reducing the likelihood of turbulent flow conditions. Turbulence can lead to inefficiencies in pump operation, resulting in increased energy consumption and potential mechanical wear. Moreover, persistent turbulence may cause severe hydrostatic pressure fluctuations and cavitation, significantly impacting the reliability and longevity of the pump system. Additionally, a detailed analysis was conducted to measure the average swirl angles across all operational pumps in each scenario, revealing average swirl angles of 3.4° for the Sym-3 scenario and 4.5° for the Asym-5 scenario.

These calculations are significant, as smaller swirl angles indicate a more aligned and stable incoming flow, which is essential for minimizing rotational flow patterns that contribute to inefficiencies. Both swirl angle values remain well within the maximum allowable limit of 7° established by the ANSI/HI 9.8-2012 standard, designed to mitigate issues related to vortex formation and the risk of cavitation during pump operations. Compliance with this standard not only maintains optimal pump performance but also enhances operational safety and equipment durability. Exceeding this limit could lead to undesirable flow conditions, including increased pressure fluctuations and vortex formation that hinder pump functionality

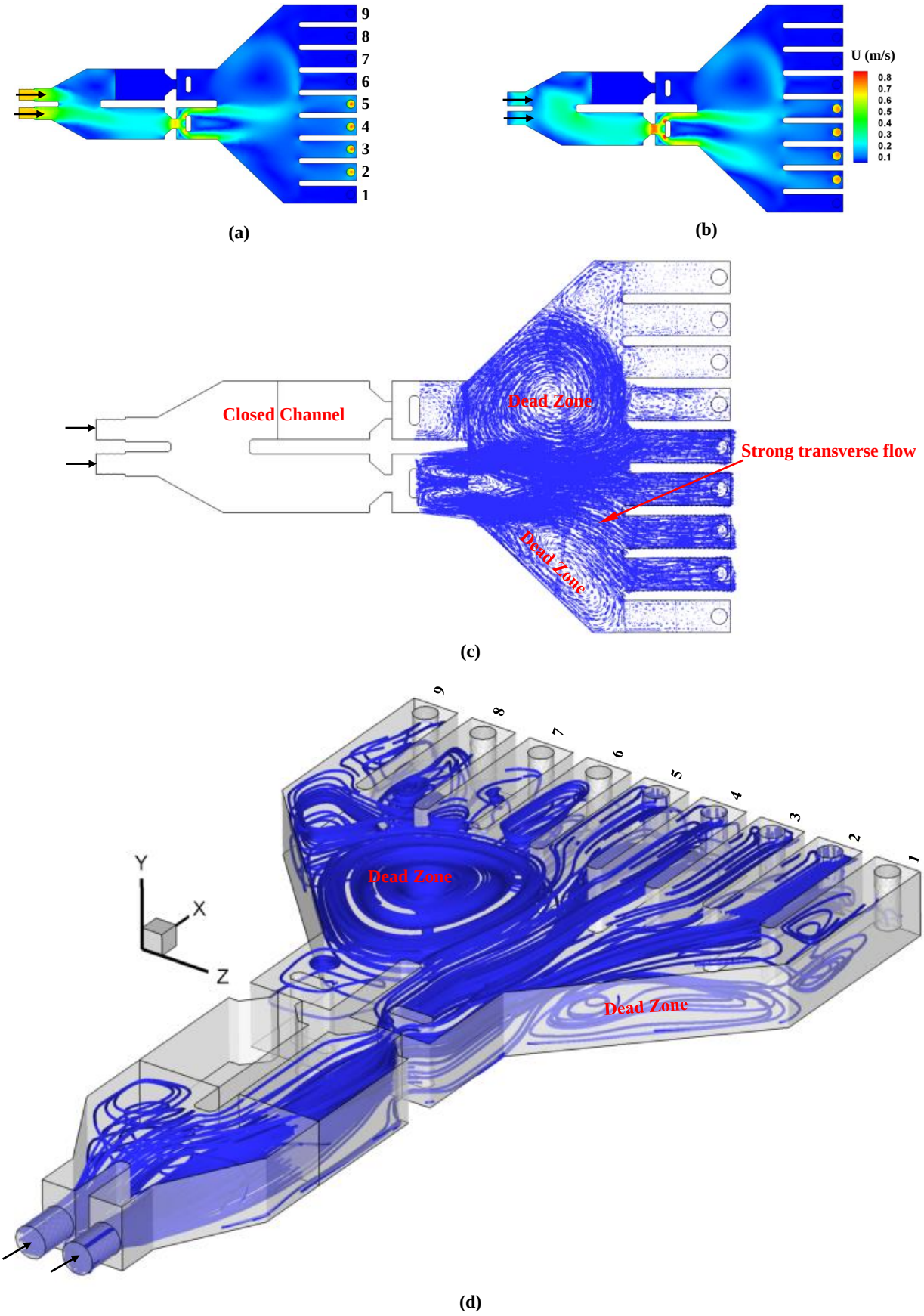

Fig. 10: Results of CFD analysis for Asym-1 scenario; (a) distribution of the velocity magnitude in Y= -5.7 m plane, (b) distribution of the velocity magnitude in Y= -2.7 m plane, (c) flow pattern in Y= -2.7 m plane, and (d) three dimensional streamlines

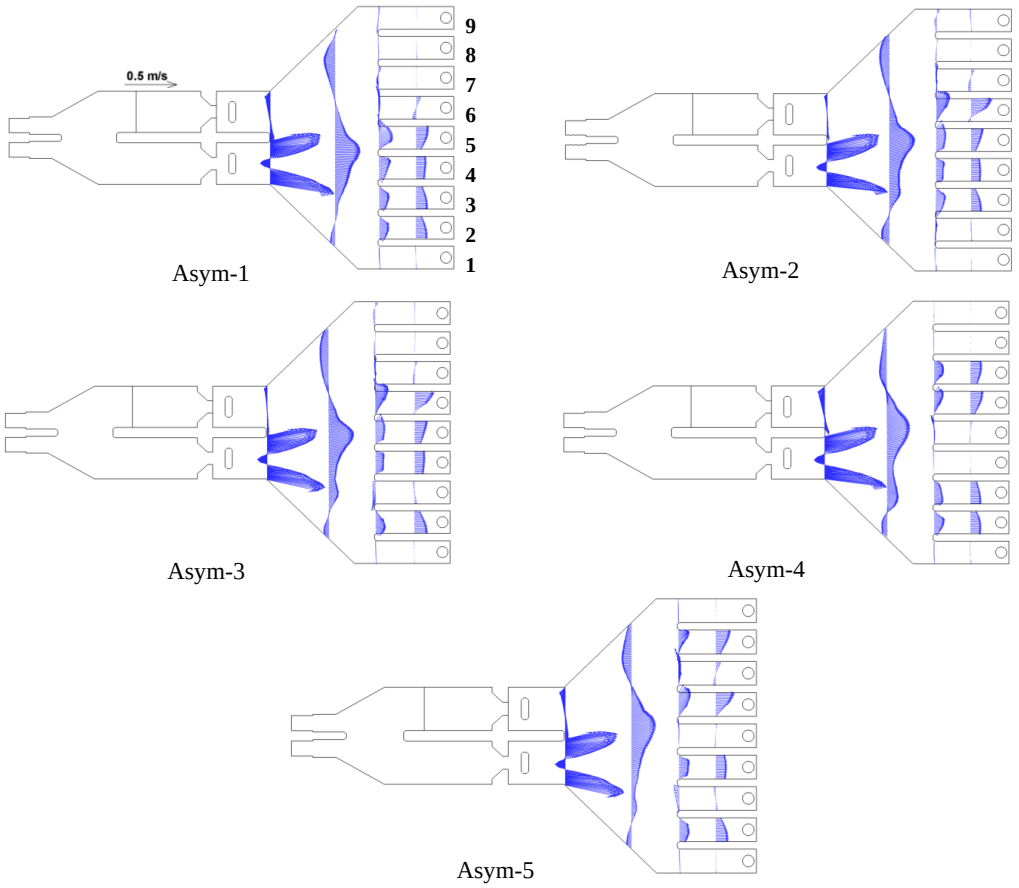

Fig. 11: Depth averaged velocity vectors for different operating scenarios of the pump intakes in the asymmetric operation mode of the basin.

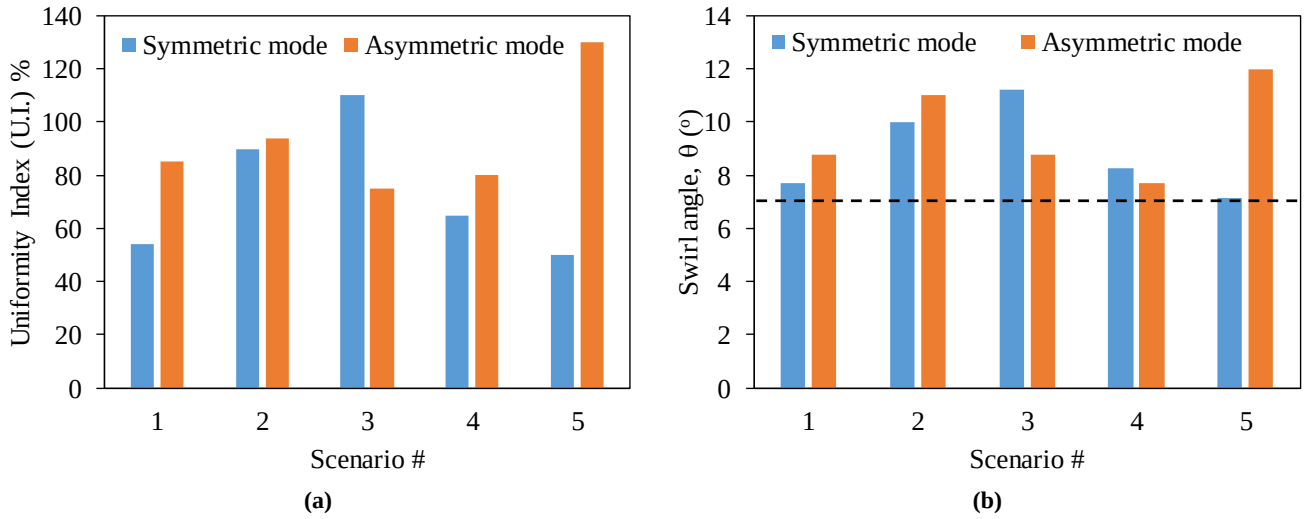

Fig. 12: Quantitative examination of the flow in the intake channels for symmetric and asymmetric operating modes; (a) calculated uniformity index for the inlet flow of the pump intakes, (b) calculated average swirl angle at the pump pipes

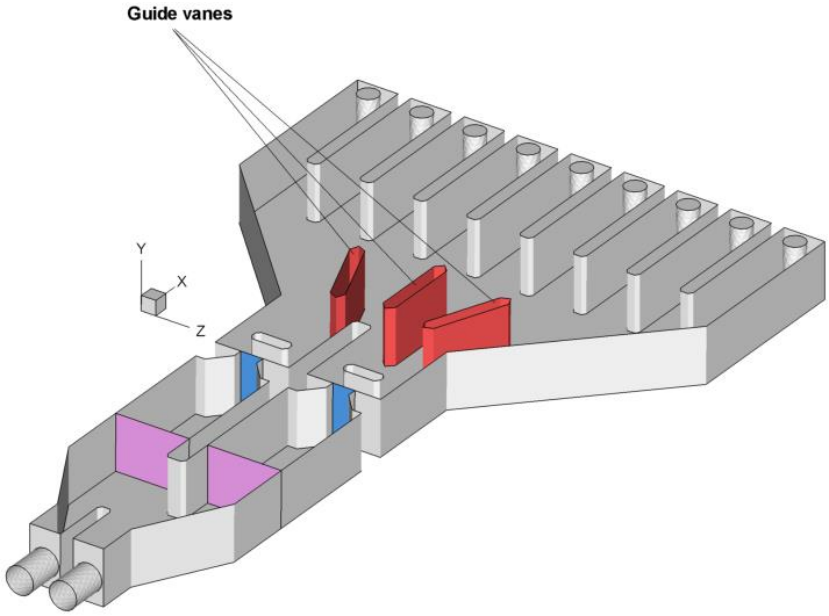

(a)

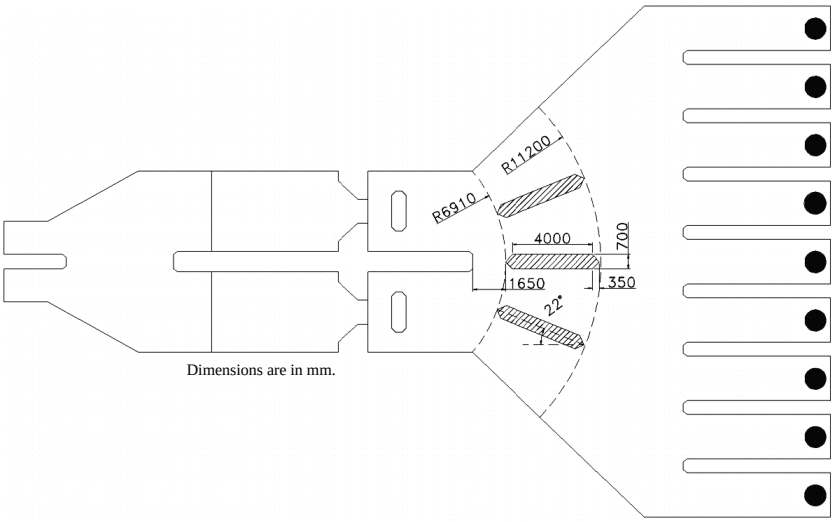

(b)

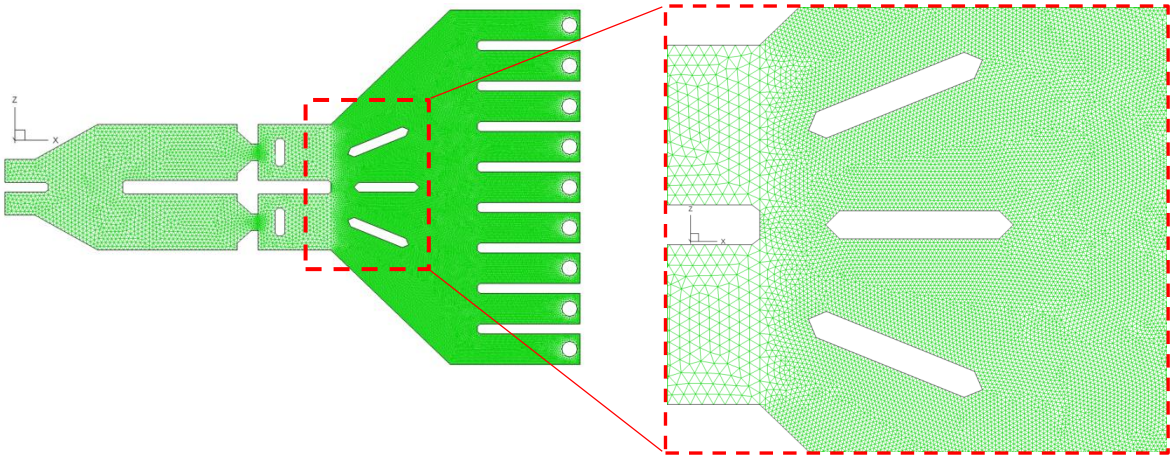

(c)

Fig. 13: Modified geometry of the Bandar Abbas seawater intake system using three guide vanes; (a) 3D geometry, (b) top view of the basin with dimensions of the guide vanes, and (c) 2D view of the computational cells

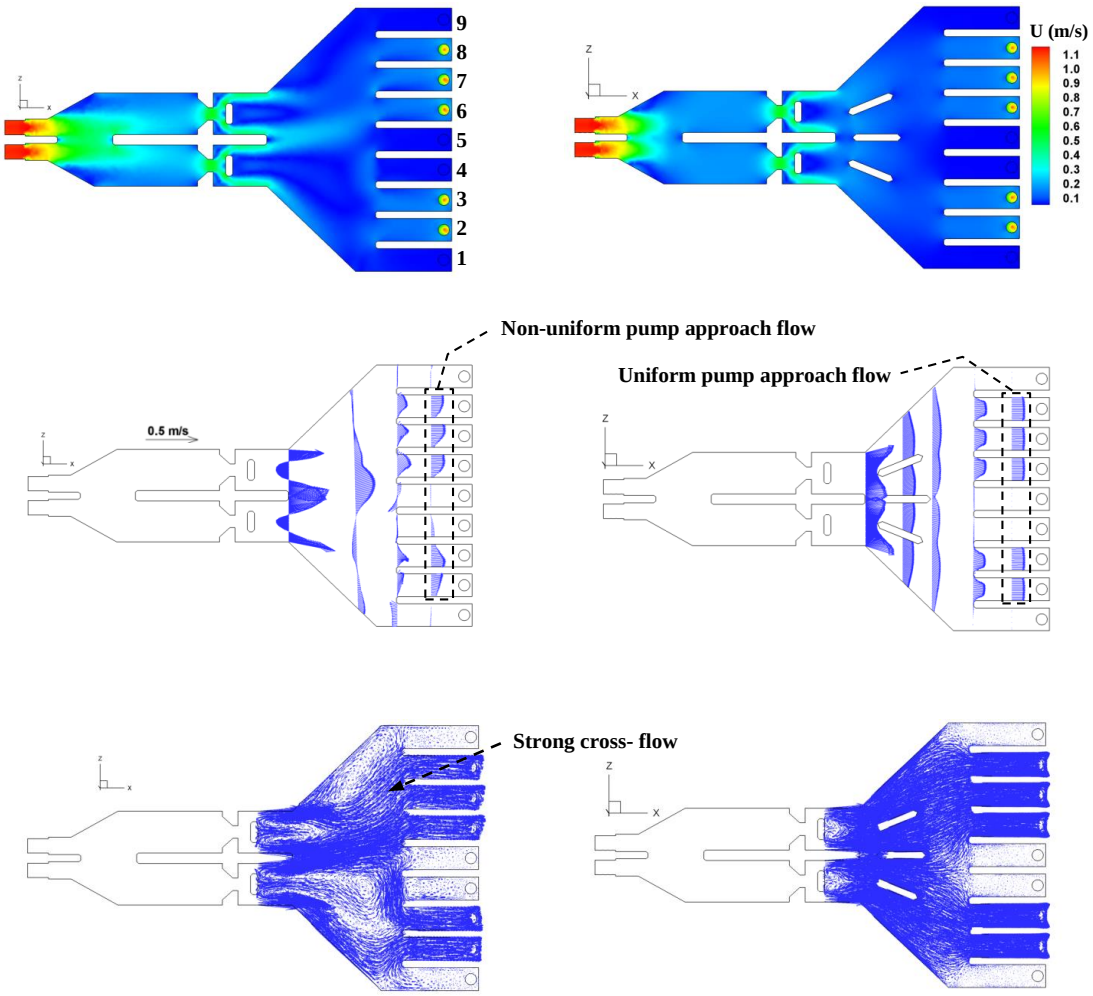

Fig. 14: Comparison of the flow field between the initial (left) and modified (right) basins in Sym-3 operating scenario.

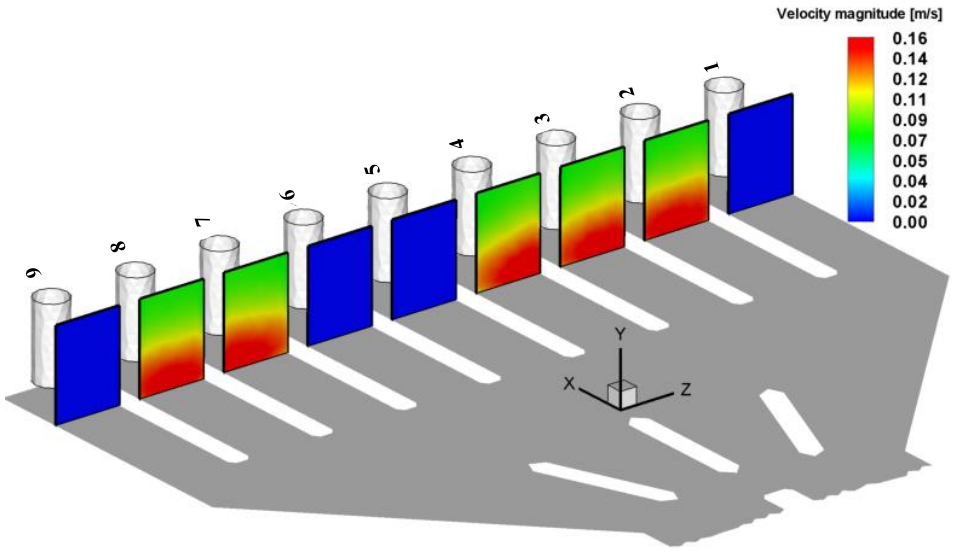

Fig. 15: Velocity magnitude contours in Sym-3 scenario for the modified geometry.

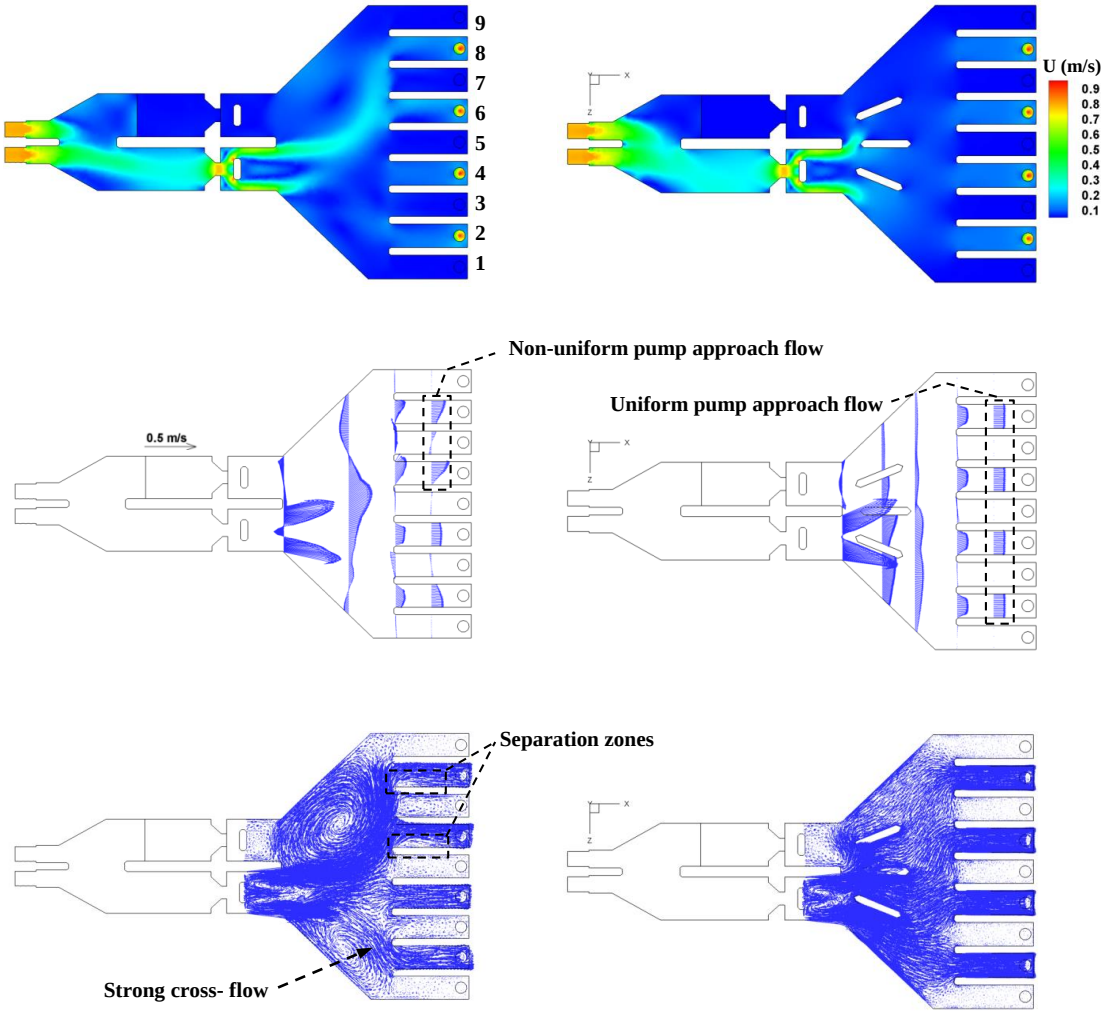

Fig. 16: Comparison of the flow field between the initial (left) and modified (right) basins in Asym-5 scenario.

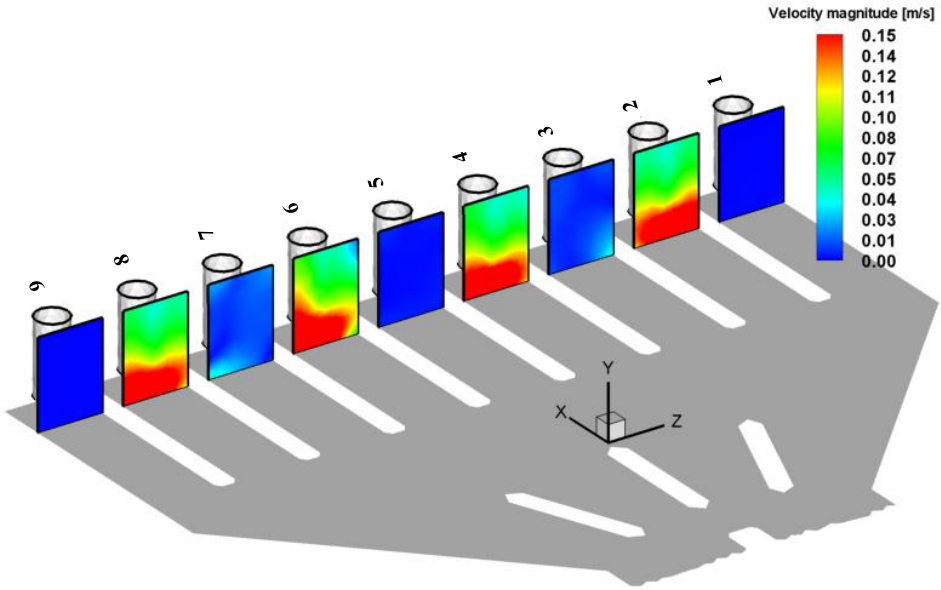

Fig. 17: Velocity magnitude contours in Asym-5 operating scenario for the modified geometry of the basin.

6.2.1 Calculation of the circulation and swirl angle along the suction pipes

To quantitatively evaluate the enhancement of the flow field in the modified basin geometry concerning vortices, we utilized circulation and swirl angle measurements of the flow within the suction pipes. The vortical structures in the basin, contribute to the circulation and swirl angle of the flow in the suction pipe. In this study the circulation (Γ) and swirl angle (φ) are determined from numerical results using a simple mathematical procedure. The circulation is defined as the line integral around a closed curve of the fluid velocity and can be related to vorticity by the Stokes theorem, which is written as [25]:

$$\Gamma = \oint_c u.dL = \iint_S (\nabla \times u).dA = \iint_S \omega.dA \qquad (7)$$

Where u represents the velocity field, A denotes the surface area vector, Γ signifies the circulation, ∇ is the divergence operator, and ω indicates the vorticity vector. As illustrated in Figure 18, to compute the circulation, the suction pipe is segmented into 20 horizontal sliced discs. Each disc is further divided into several small elements, and the average vorticity (ω_i) is calculated for its corresponding area (A_i). Equation (6) is substituted with the following simplified summation to determine the total circulation at each cross-section :

$$\Gamma \approx \sum_{i=1}^{n} |\omega_i| A_i \qquad (8)$$

The circulation is normalized by the pipe velocity and its diameter, expressed as follows:

$$\Gamma^+ = \frac{1}{U_p D} \sum_{i=1}^{n} |\omega_i| A_i \qquad (9)$$

Assuming that the pipe flow behaves as a forced vortex, the mean angular velocity of a disk (U_θ) and the swirl angle (φ) can be calculated using the circulation as follows:

$$U_\theta = \frac{\Gamma}{\pi D} \qquad (10)$$

$$\varphi = tan^{-1}\left(\frac{U_\theta}{U_p}\right) = tan^{-1}\left(\frac{\Gamma}{\pi D U_p}\right) \qquad (11)$$

Figure 19 illustrates the vertical variations of circulation and swirl angle along suction pipe #8 for both the base and modified basins in Sym-3 scenario. The vertical axis, $y^+ = y/D$ represents the normalized distance from the floor.

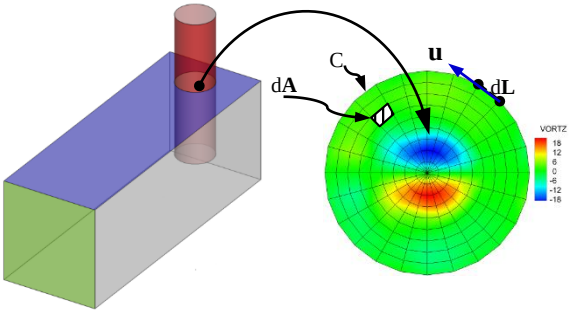

Fig. 18: Diagram of how to obtain circulation on each selected disc along the suction pipe using surface integral of the vorticity field.

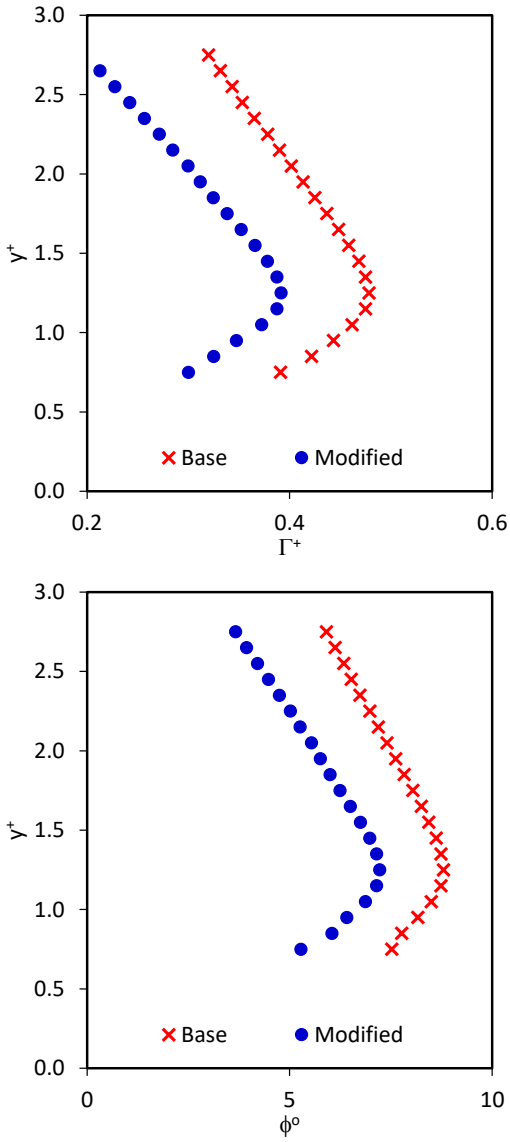

Fig. 19: Vertical variations of circulation and swirl angle along suction pipe #8 for the base and modified geometries in Sym-3 scenario.

Based on the hydraulic model studies, Ansar recommended that the maximum acceptable magnitude of the swirl angle

is 5° [28]. Figure 19(b) shows that the swirl angle is higher than 5° in the entire length of the suction pipe. The maximum swirl angle is 8.7° and it occurs similar to the rotation maxima at y^+=1.25 level. In contrast to the base geometry, the rotation angle in most parts of the suction pipe in the modified geometry is less than 5 degrees. This indicates compliance with the recommended conditions outlined in ANSI 9.8.

These differences are attributed to the non-uniformity of the approaching flow along the intake channel, which arises from the formation of vortices and circulating regions in the embayment area.

7. Conclusions

The objective of this research was to employ numerical simulations to investigate the hydrodynamic behavior of the intake system at the Bandar Abbas seawater desalination facility, a critical infrastructure for providing potable water. This study aimed to provide a comprehensive analysis of the flow dynamics associated with the intake system, which is essential in ensuring efficient operation and optimal performance of the desalination process. To achieve this, the investigation considered both symmetric and asymmetric operational modes of the intake system, which are often encountered in practical applications due to variations in demand and operational constraints. The research rigorously assessed the influence of different pump operating scenarios on the flow field within the forebay region and along the pump bays. By simulating various configurations and operational parameters, the study sought to identify the conditions that could lead to flow inefficiencies and potential operational challenges.

The results of the simulations revealed that the initial design of the forebay exhibited multiple stagnant zones, which significantly affected the flow characteristics. These dead zones contributed to flow non-uniformity and the formation of separation zones along the pump bays. Such conditions can adversely impact the overall efficiency of the intake system, leading to potential cavitation in pumps and reduced effective flow rates. Furthermore, the study found that the asymmetric operation of the intake system further exacerbated these detrimental flow conditions, highlighting the need for design modifications to ensure consistent, efficient operation.

In light of these findings, the research proposed geometric modifications to the basin design. Specifically, the introduction of three diverging guide vanes at the forebay inlet was simulated to evaluate its effectiveness in improving the flow dynamics. The modifications aimed to redirect the incoming flow more efficiently and mitigate the adverse effects observed in the initial design. The results indicated a significant improvement in flow patterns ; the implementation of these guide vanes successfully eliminated all stagnant zones, facilitating a more uniform flow distribution across all pump bays. This enhanced flow regime not only improved operational reliability but also minimized the risk of flow-induced issues, such as separation zones that could lead to performance degradation. Moreover, the modified geometric configuration met all recommendations set forth in the ANSI/HI 9.8-2012 standard, which outlines best practices for pump intake design. These adjustments not only promote optimal hydraulic performance but also contribute to the long-term sustainability of the desalination plant's operations by enhancing energy efficiency and reducing maintenance requirements. Overall, this research underscores the significance of hydrodynamic analysis and design optimization in the improvement of seawater desalination systems, providing valuable insights for future studies and practical applications in the field.

References

[1] Ayaz, M., Namazi, M. A., ud Din, M. A., Ershath, M. M., & Mansour, A. (2022). Sustainable seawater desalination: current status, environmental implications and future expectations. *Desalination*, 540, 116022. https://doi.org/10.1016/j.desal.2022.116022

[2] Pulido-Bosch, A., Vallejos, A., & Sola, F. (2019). Methods to supply seawater to desalination plants along the spanish mediterranean coast and their associated issues. *Environmental Earth Sciences*, 78, 1-9. https://doi.org/10.1007/s12665-019-8298-9

[3] Elsaid, K., Kamil, M., Sayed, E. T., Abdelkareem, M. A., Wilberforce, T., & Olabi, A. (2020). Environmental impact of desalination technologies: a review. *Science of the Total Environment*, 748, 141528. https://doi.org/10.1016/j.scitotenv.2020.141528

[4] ANSI/HI 9.8-2012; American National Standards Institute. (2012). American National Standard for Rotodynamic Pumps for Pump Intake Design. Hydraulic Institute.

[5] Mitra, P., Gudibande, N., Iyer, K., & Eldho, T. I. (2015). Algorithm for estimating swirl angles in multi-intake hydraulic sumps. *arXiv preprint arXiv*:1509.01709.

[6] Gordon, J. (1970). Vortices at intakes. *Journal of Water Power*, 22(4)**,** 137-138.

[7] Constantinescu, G. S. & Patel, V. C. (1998). Numerical model for simulation of pump-intake flow and vortices. *Journal of Hydraulic Engineering*, 124(2), 123-134. https://doi.org/10.1061/(ASCE)0733-9429(1998)124:2(123)

[8] Ansar, M. & Nakato, T. (2001). Experimental study of 3D pump-intake flows with and without cross flow. *Journal of Hydraulic Engineering*, 127(10)**,** 825-834. https://doi.org/10.1061/(ASCE)0733-9429(2001)127:10(825)

[9] Hwang, K. S. & Yang, C. H. (2003). Hydraulics model testing of circulating-water pump sump in Shen-Ho power plant. Research Report 293. Taiwan Hydraulics Laboratory, Tainan.

[10] Li, S., Lai, Y., Weber, L., Silva, J. M., & Patel, V. C. (2004). Validation of a three-dimensional numerical model for water-pump intakes. *Journal of Hydraulic Research*, 42(3), 282-292. https://doi.org/10.1080/00221686.2004.9728393

[11] Tokyay, T. E., & Constantinescu, S. G. (2006). Validation of a large-eddy simulation model to simulate flow in pump intakes of realistic geometry. *Journal of hydraulic Engineering*, 132(12), 1303-1315.https://doi.org/10.1061/(ASCE)0733-9429(2006)132:12(1303)

[12] Issa, A., Bayeul-Lainé, A. C., & Bois, G. (2008, October). Numerical simulation of flow field formed in water pump-sump. In 24th Symposium on Hydraulic Machinery and Systems. Foz Do Iguassu, Brazil.

[13] Chuang, W. L., Hsiao, S. C., & Hwang, K. S. (2014). Numerical and experimental study of pump sump flows. *Mathematical problems in engineering*, 2014. https://doi.org/10.1155/2014/735416

[14] Kim, C. G., Choi, Y. D., Choi, J. W. & Lee, Y. H. (2010). A Study on the effectiveness of an anti-vortex device in the sump model by experiment and CFD. *In 26th IAHR Symposium on Hydraulic Machinery and Systems*. Beijing, China.

[15] Safarzadeh, A., Talebi, M., & Mohajeri, S. H. (2020). Numerical study of the surface and subsurface vortices suppression in a rectangular pump basin using anti-vortex devices. *Water and Environment Journal*, 34, 454-467. https://doi.org/10.1111/wej.12545

[16] Zhang, C., Yan, H., Jamil, M. T., & Yu, Y. (2022). Improvement of the flow pattern of a forebay with a side-intake pumping station by diversion piers based on orthogonal test method. *Water*, 14(17), 2663. https://doi.org/10.3390/w14172663

[17] Song, X. J., Yao, R., Chao, L., & Wang, Z. W. (2021). Study of the formation and dynamic characteristics of the vortex in the pump sump by CFD and experiment. *Journal of Hydrodynamics*, 33 (6), 1202–1215. https://doi.org/10.1007/s42241-021-0095-8

[18] Choi, J. W., Choi, Y. D., Kim, C. G., & Lee, Y. H. (2010). Flow uniformity in a multi-intake pump sump model. *Journal of Mechanical Science and Technology*, 24 (7), 1389-1400. https://doi.org/10.1007/s12206-010-0413-5

[19] Dimas, A. A., & Vouros, A. P. (2012). Effect of cross-flow velocity at forebay on swirl in pump suction pipe: Hydraulic model of seawater intake at Aliveri Power Plant in Greece. *Journal of Hydraulic Engineering*, 138(9), 812-816. https://doi.org/10.1061/(ASCE)HY.1943-7900.0000576

[20] Nasr, A., Yang, F., Zhang, Y., Wang, T., & Hassan, M. (2021). Analysis of the flow pattern and flow rectification measures of the side-intake forebay in a multi-unit pumping station. *Water*, 13 (15), 2025. https://doi.org/10.3390/w13152025

[21] Longo, D., Dimakopoulos, A., & Willoughby, I. (2022). Numerical modelling of pump intakes: compliance with standard performance criteria. Proceedings of the 39th IAHR World Congress. Granada, Spain.

[22] Zhang, W., Tang, F., Shi, L., Hu, Q., & Zhou, Y. (2020). Effects of an inlet vortex on the performance of an axial-flow pump. *Energies*, 13(11), 2854. https://doi.org/10.3390/en13112854

[23] Yamini, O. A., Movahedi, A., Mousavi, S. H., Kavianpour, M. R., & Kyriakopoulos, G. L. (2022). Hydraulic performance of seawater intake system using CFD modeling. *Journal of Marine Science and Engineering*, 10(7), 988. https://doi.org/10.3390/jmse10070988

[24] Celik, I., & Rodi, W. (1984). Simulation of free-surface effects in turbulent channel flows. *Physicochemical Hydrodynamics*, 5(3-4), 217-227.

[25] Safarzadeh, A., & Brevis, W. (2016). Assessment of 3D-RANS models for the simulation of topographically forced shallow flows. *Journal of Hydrology and Hydromechanics*, 64(1), 83-90. https://doi.org/10.1515/johh-2016-0008

[26] Launder, B.E. (1989). Second-moment closure and its use in modeling turbulent industrial flows. *International Journal of Numerical Methods in Fluids*, 9, 963–985. https://doi.org/10.1002/fld.1650090806

[27] Leschziner, M. A., & Rodi, W. (1979). Calculation of strongly curved open channel flow. *Journal of the Hydraulics Division*, 105(10), 1297-1314. https://doi.org/10.1061/JYCEAJ.0005286

[28] Ansar, M. (1997). Experimental and theoretical studies of pump-approach flow distributions at water intakes. The University of Iowa.